DEVELOPMENTAL BIOLOGY

Apical cell expansion maintained by Dusky-like establishes a scaffold for corneal lens morphogenesis

Neha Ghosh and Jessica E. Treisman*

The *Drosophila* corneal lens is entirely composed of chitin and other apical extracellular matrix components, and it is not known how it acquires the biconvex shape that enables it to focus light onto the retina. We show here that the zona pellucida domain–containing protein Dusky-like is essential for normal corneal lens morphogenesis. Dusky-like transiently localizes to the expanded apical surfaces of the corneal lens-secreting cells and prevents them from undergoing apical constriction and apicobasal contraction. Dusky-like also controls the arrangement of two other zona pellucida domain proteins, Dumpy and Piopio, external to the developing corneal lens. Loss of either *dusky-like* or *dumpy* delays chitin accumulation and disrupts the outer surface of the corneal lens. We find that artificially inducing apical constriction by activating myosin contraction is sufficient to similarly alter chitin deposition and corneal lens morphology. These results demonstrate the importance of cell shape in controlling the morphogenesis of overlying apical extracellular matrix structures such as the corneal lens.

INTRODUCTION

The extracellular matrix (ECM) is a complex array of proteins and polysaccharides that provides structural and biochemical support to tissues. Mutations affecting the ECM can cause numerous human genetic disorders including cancer, muscular dystrophy, hematuria, and retinopathy (*1*–*3*). Basement membrane ECM, which forms a sheet underlying epithelial cells, is made up of conserved proteins such as collagen, nidogen, perlecan, and laminins. It can mediate adhesion between tissue layers, insulate cells from the extracellular fluid, transmit mechanical forces, influence the distribution of signaling molecules, and act as a substrate for cell migration (*3*–*5*). Less is known about the apical ECM (aECM), which has diverse forms and functions. External aECMs such as invertebrate cuticles can act as permeability barriers and protect against desiccation, and the shapes of tubular organs such as the *Drosophila* trachea and *Caenorhabditis elegans* excretory system depend on luminal scaffolds composed of aECM (*6*, *7*). In vertebrates, aECM forms structures such as the tectorial membrane of the inner ear, the vascular glycocalyx, pulmonary surfactant, and the mucin-rich lining of the gut (*8*–*11*). The morphogenesis of aECM assemblies is not fully understood, although in a few cases, it has been linked to cytoskeletal organization in the underlying cells (*12*, *13*).

One of the most remarkable structures composed of aECM is the *Drosophila* corneal lens, which consists of fibers of the polysaccharide chitin and associated proteins arranged to form a precisely curved biconvex shape that can focus light onto the underlying photoreceptors (*14*, *15*). The corneal lens of each ommatidium of the compound eye is secreted during the second half of pupal development by the underlying nonneuronal cells (*16*). Major corneal lens constituents such as Crystallin are produced by the central cone and primary pigment cells, while additional components are derived from the secondary and tertiary pigment cells attached to the corneal lens periphery (*14*, *17*). Although it is not known how these cells specify the shape of the corneal lens, we have previously shown that the transcription factor Blimp-1 is essential to generate its outer curvature (*18*). Many Blimp-1 target genes encode aECM components, including members of the most conserved family of aECM proteins, which are characterized by a zona pellucida (ZP) domain (*18*, *19*).

The ZP domain was initially identified in constituents of the extracellular coat surrounding the mammalian oocyte (*20*), but has since been found in proteins implicated in many developmental processes (*19*). Mutations affecting human ZP-domain proteins are associated with disease conditions that include infertility, deafness, vascular disorders, inflammatory bowel disease, kidney disease, and cancer (*21*–*26*). The 260–amino acid ZP domain can mediate homomeric or heteromeric polymerization into filaments; it consists of N- and C-terminal subdomains with structures related to immunoglobulin domains that are stabilized by conserved disulfide bonds (*27*–*29*). Some ZP-domain proteins are tethered to the plasma membrane by a transmembrane domain or GPI linkage, while others undergo proteolytic cleavage and are secreted into the extracellular space (*30*–*33*).

ZP-domain proteins have been found to play a crucial role in shaping the aECM and attaching it to the apical plasma membrane (*7*, *19*). For instance, the α-tectorin ZP-domain protein is essential for attachment of the tectorial membrane to the cochlear epithelium (*34*). Filaments of the giant *Drosophila* ZP-domain protein Dumpy (Dpy) anchor pupal appendages and tendon cells to the external cuticle (*35*–*37*), and the dendrites of sensory organs also require ZP-domain proteins to connect them to the cuticle (*33*, *38*). The lumen of tubular structures in *Drosophila, C. elegans*, and the mammalian kidney is organized by ZP-domain proteins (*26*, *39*–*41*). Mutations affecting eight *Drosophila* ZP-domain proteins each have distinct effects on the morphology of embryonic denticles, and each protein occupies a specific spatial location in the denticle (*42*), indicating that ZP-domain proteins are specialized to assemble aECM into diverse shapes.

Here, we show that the ZP-domain protein Dusky-like (Dyl) (*42*–*44*) is essential for normal morphogenesis of the *Drosophila* corneal lens. During pupal development, *dyl* mutant ommatidia undergo abnormal apical constriction and apicobasal contraction accompanied by changes in the distribution of cytoskeletal proteins. Loss of *dyl* also results in changes in the organization of other ZP-domain proteins such as Dpy and Piopio (Pio) (*32*, *39*, *45*) and a delay in the accumulation of chitin. Many of these changes can be phenocopied by activating myosin to artificially induce constriction of the corneal lens-secreting cells. These observations suggest that

Department of Cell Biology, NYU Grossman School of Medicine, 540 First Avenue, New York, NY 10016, USA.
*Corresponding author. Email: jessica.treisman@nyulangone.org

Dyl maintains the expanded apical surface area of cone and primary pigment cells, perhaps by transiently attaching them to the aECM, and thus enables the generation of a ZP-domain protein scaffold that shapes the curved corneal lens surface.

RESULTS

Dyl is necessary for normal corneal lens morphology

The *Drosophila* corneal lens is a biconvex aECM structure that focuses light onto the underlying photoreceptors (*15*). The transcription factor Blimp-1 is necessary for normal corneal lens curvature, and its target genes include several that encode ZP-domain proteins (*18*). ZP-domain proteins have been reported to connect aECM to the plasma membrane of epithelial cells, and mutations affecting these proteins can alter the shape of cuticular structures such as embryonic denticles (*42*) and bristles (*43*, *44*). We therefore used existing mutants and RNAi lines to test whether any ZP-domain targets of Blimp-1 were necessary for the normal shape of the corneal lens.

We observed a marked effect on the external appearance of the adult eye in clones mutant for one such gene, *dyl*. Scanning electron micrographs showed that in ommatidia homozygous for $dyl^{\Delta 42}$, a deletion of the entire gene (*42*), the corneal lenses lacked external curvature and had gaps in their outer surfaces (Fig. 1, A and B). The same flat shape and abnormal surface structure were visible in transmission electron micrographs (fig. S1, A and B). Cryosections of eyes stained for chitin with Calcofluor White revealed that the flatter external surfaces of the *dyl* mutant corneal lenses were accompanied by more deeply curved internal surfaces than those of the adjacent wild-type biconvex corneal lenses (Fig. 1, E and F). Quantification of the outer and inner angles between adjacent corneal lenses (Fig. 1I) confirmed that the outer angle was significantly increased and the inner angle significantly decreased in *dyl* mutant regions (Fig. 1, J and K). The changes in corneal lens shape observed in $dyl^{\Delta 42}$ mutants, which included increased height and reduced width, were rescued by expression of a *UAS-dyl* transgene (*42*) in all retinal cells with *lGMR-GAL4* (*46*), confirming that the defects were due to loss of *dyl* (Fig. 1, C, D, G, H, J, and K, and fig. S1, E and F). In transmission electron micrographs, we observed that the deeper inner curvature of the corneal lens correlated with an increase in its area of contact with the peripheral secondary and tertiary pigment cells (fig. S1, A to D and G). Together, our results show that the ZP-domain protein Dyl is necessary for the normal biconvex shape and external morphology of the corneal lens.

Loss of *dyl* causes apical constriction and apico-basal contraction of ommatidia

To understand how loss of *dyl* affects corneal lens shape, we traced the mutant phenotype earlier in development. Corneal lens secretion initiates at 50 hours after puparium formation (APF) and continues through

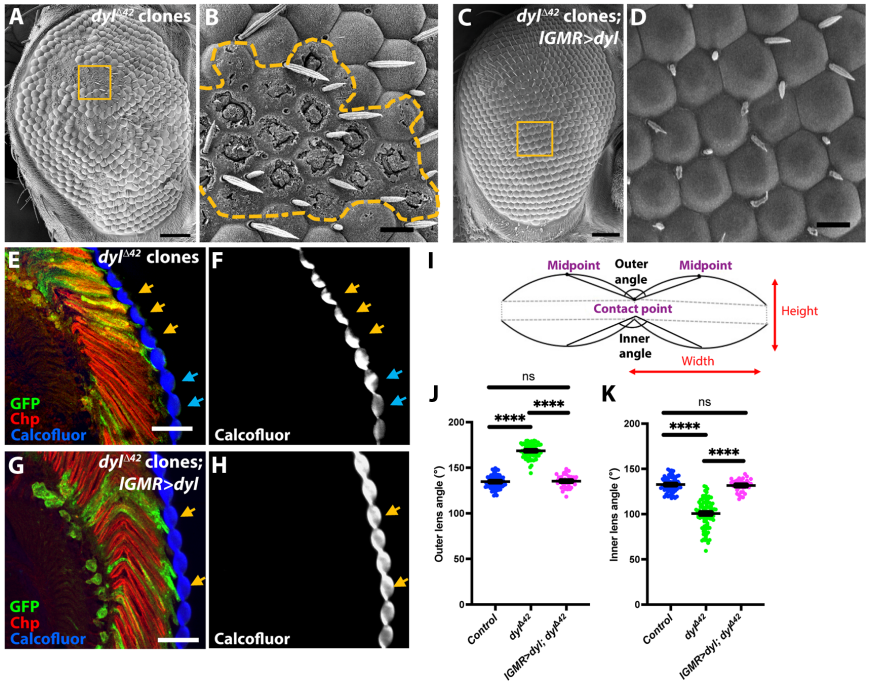

Fig. 1. *dyl* is necessary for normal corneal lens curvature. (**A** to **D**) Scanning electron micrographs of adult eyes. (A) and (B) In $dyl^{\Delta 42}$ mutant clones, the corneal lens surfaces are flat rather than convex, and many appear to be missing parts of the surface layer. (C) and (D) Expressing a *UAS-dyl* transgene with *lGMR-GAL4* in $dyl^{\Delta 42}$ mutant clones restores their external surface structure. The regions in the yellow boxes in (A) and (C) are enlarged in (B) and (D), and the boundaries of the *dyl* mutant clone are marked with a yellow dotted line in (B). (**E** to **H**) Horizontal frozen sections of adult eyes in which $dyl^{\Delta 42}$ mutant clones [(E) and (F)] or $dyl^{\Delta 42}$ mutant clones expressing *UAS-dyl* with *lGMR-GAL4* [(G) and (H)] are positively marked with GFP (green). The corneal lenses are stained with Calcofluor White [(F) and (H); blue in (E) and (G)] and photoreceptors are marked with anti-Chaoptin (Chp, red). *dyl* mutant ommatidia have externally flat corneal lenses [yellow arrows, (E) and (F)] while adjacent wild-type ommatidia have biconvex corneal lenses [blue arrows, (E) and (F)]. Rescue with *UAS-dyl* restores the normal corneal lens shape [yellow arrows, (G) and (H)]. (**I**) Schematic illustration showing how the outer and inner angles between adjacent corneal lenses and the height and width of a corneal lens were defined. (**J** and **K**) Graphs showing the outer (J) and inner (K) angles between adjacent corneal lenses in adult eye sections for wild-type control regions, $dyl^{\Delta 42}$ mutant clones, and $dyl^{\Delta 42}$ mutant clones in which *UAS-dyl* is driven with *lGMR-GAL4*. For both graphs, error bars show mean ± SEM. *n* values are given as number of ommatidia/number of retinas for this and subsequent graphs. Wild type $n = 70/20$, *dyl* $n = 103/20$, *lGMR > dyl*; *dyl* $n = 37/6$. ****$P < 0.0001$, unpaired two-tailed *t* test with Welch's correction. Scale bars, 40 μm [(A) and (C)], 10 μm [(B) and (D)], and 20 μm [(E) and (G)].

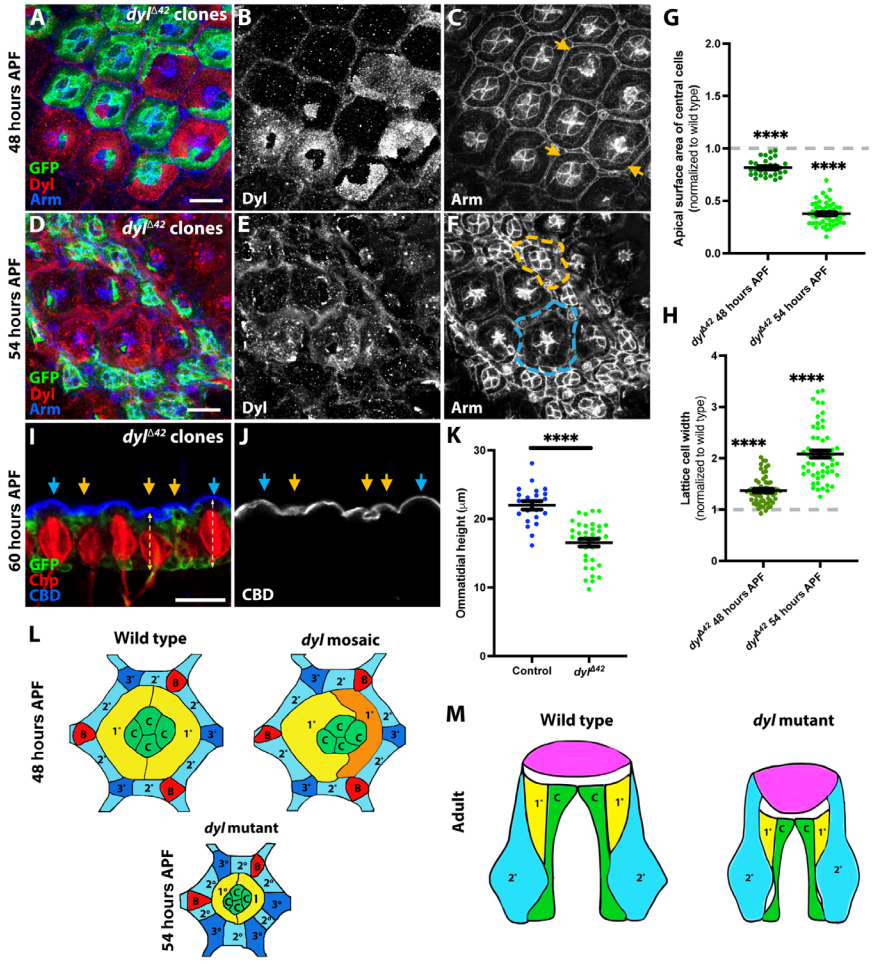

Fig. 2. Loss of *dyl* causes apical constriction and apico-basal contraction of ommatidia. (**A** to **F**) Retinas containing $dyl^{\Delta 42}$ clones marked with GFP (green), stained for Dyl [(B) and (E), red in (A) and (D)] and Arm [(C) and (F), blue in (A) and (D)] at 48 hours APF [(A) to (C)] or 54 hours APF [(D) to (F)]. $dyl^{\Delta 42}$ clones show loss of Dyl staining in central cells, reduced apical surface area, and apicobasal contraction [yellow arrows, (C); yellow outline, (F)], compared to wild-type ommatidia (blue outline, F). (**G** and **H**) Graphs depicting central cell apical surface area (G) or lattice cell width (H) in $dyl^{\Delta 42}$ clones, normalized to wild-type ommatidia in the same retinas, at 48 hours APF [(G): $n = 28/18$ (control), 32/18 (*dyl*), (H): $n = 69/7$ (control), 61/7 (*dyl*)] and 54 hours APF [(G): $n = 44/27$ (control), 52/12 (*dyl*), (H): $n = 37/7$ (control), 57/7 (*dyl*)]. (**I** and **J**) Horizontal cryosection of a 60-hour APF retina showing apicobasal contraction in $dyl^{\Delta 42}$ clones marked with GFP (green, yellow arrows) relative to wild-type ommatidia (blue arrows). Alexa647-labeled CBD [(J), blue in (I)] marks the corneal lenses, and anti-Chp (red) stains photoreceptor rhabdomeres. Dotted lines show ommatidial height. Scale bars, 10 μm [(A) to (F)] and 20 μm [(I) and (J)]. (**K**) Graph showing ommatidial height in $dyl^{\Delta 42}$ clones and wild-type ommatidia at 60 hours APF [$n = 21/5$ (control), 35/5 (*dyl*)]. For all graphs, error bars show mean ± SEM. $^{****}P < 0.0001$, one-sample *t* test and Wilcoxon test [(G) and (H)] or unpaired two-tailed *t* test with Welch's correction (K). (**L**) Diagrams of wild-type and *dyl* mosaic ommatidia at 48 hours APF and a *dyl* mutant ommatidium at 54 hours APF. Cone cells (C) and primary pigment cells (1°) are surrounded by secondary pigment cells (2°), tertiary pigment cells (3°), and mechanosensory bristles (B). (**M**) Schematic of horizontal views of wild-type and *dyl* mutant adult ommatidia, showing altered corneal lens shape (pink).

the late pupal stages (*16*). Major components of the corneal lens such as Crystallin and Retinin are produced by the underlying cone and primary pigment cells, and additional constituents are secreted by the secondary and tertiary pigment cells (also called lattice cells, Fig. 2L) (*14*). To determine the site of Dyl expression in the retina, we used an antibody against Dyl (*42*), and identified specific labeling by its absence in *dyl* mutant clones (Fig. 2, A to F, and fig. S2, A to F; lattice cells showed nonspecific staining). We observed that Dyl was present on the apical surface of the cone and primary pigment cells at 48 hours APF (Fig. 2, A to C) and 50 hours APF (fig. S2, A to C). Dyl protein levels were reduced at 52 hours APF (fig. S2, D to F) and became very low at 54 hours APF (Fig. 2, D to F), consistent with the transient 48 hours APF peak of *dyl* mRNA reported by modENCODE (*47*).

dyl mutant ommatidia showed a notable apical constriction, visualized by staining apical adherens junctions for Armadillo (Arm, β-catenin), which started at 48 hours APF (Fig. 2, A to C) and became very pronounced at 54 hours APF (Fig. 2, D to F, and fig. S2L). The change was driven by a large decrease in the apical surface area of the cone and primary pigment cells (together known as the central cells) (Fig. 2G); in contrast, the apical width of the lattice cells expanded (Fig. 2H). The apical constriction of *dyl* mutant ommatidia was accompanied by apical-basal contraction, placing their apical surfaces in a deeper plane than the wild-type ommatidia at 54 hours APF (Fig. 2, D to F, compare *dyl* mutant ommatidium outlined in yellow to wild-type ommatidium outlined in blue). This change could also be visualized in cryosections of 60 hours APF pupal retinas, in which $dyl^{\Delta 42}$ ommatidia were shorter than their wild-type neighbors (Fig. 2, I to K). In these sections, the wild-type corneal lenses labeled with a fluorescent chitin-binding domain (CBD) had convex outer surfaces, whereas corneal lenses corresponding to *dyl* clones were flat or

convoluted (Fig. 2, I and J). Expression of the wild-type UAS-*dyl* transgene rescued both the apical constriction and apicobasal contraction displayed by $dyl^{\Delta 42}$ mutants (fig. S2, G to L). To examine whether loss of *dyl* affects the contacts between the apical plasma membrane and the aECM, we examined eyes containing *dyl* mutant clones using transmission electron microscopy at 72 hours APF. Wild-type ommatidia identified by normal curvature of the corneal lens had darkly stained indentations in the plasma membrane that appeared to be connected to fibers in the cytoplasm (fig. S2, M and N). In contrast, ommatidia likely to be *dyl* mutant because of their flattened corneal lenses had few such structures (fig. S2, O and P), suggesting that *dyl* promotes the formation of organized contact sites.

Together, these data suggest that Dyl acts at the apical surfaces of cone and primary pigment cells to connect them to the aECM and thus maintain their apical expansion (Fig. 2L). *dyl* mutant ommatidia or individual mutant cells in mosaic ommatidia show marked apical constriction (Fig. 2L). The corneal lens may maintain its attachment to the lattice cells as the ommatidium contracts basally, flattening its external curvature and deepening its internal curvature (Fig. 2M).

Loss of *dyl* causes cytoskeletal reorganization

We next investigated how the organization of the cytoskeleton was affected in *dyl* mutant clones. Using the actin-binding domain of the ERM protein Moesin (Moe) tagged with mCherry (*48*) to label actin filaments, we found that at 60 hours APF, Moe::mcherry was more concentrated at the apical surface of *dyl* mutant ommatidia than in neighboring wild-type ommatidia (Fig. 3, A and B). *dyl* mutant cells did not appear to contain an increased amount of Moe::mcherry (fig. S3, A to C), implying that their actin cytoskeleton is condensed into a smaller area. Actomyosin contraction can be induced by phosphorylation of the nonmuscle myosin II regulatory light chain, known in *Drosophila* as Spaghetti squash (Sqh) (*49*). We stained $dyl^{\Delta 42}$ clones in the pupal retina with an antibody against phospho-Sqh (pSqh) (*50*) and found it to be enriched in lattice cells at 50 hours APF in both wild-type and *dyl* mutant regions (fig. S3, D and E). At 54 hours APF, pSqh was present in discrete foci at the apical surfaces of wild-type cone and primary pigment cells, whereas in $dyl^{\Delta 42}$ clones, pSqh was more uniformly distributed (Fig. 3, C, D, G, and H). Loss of *dyl* had a similar effect on the distribution of

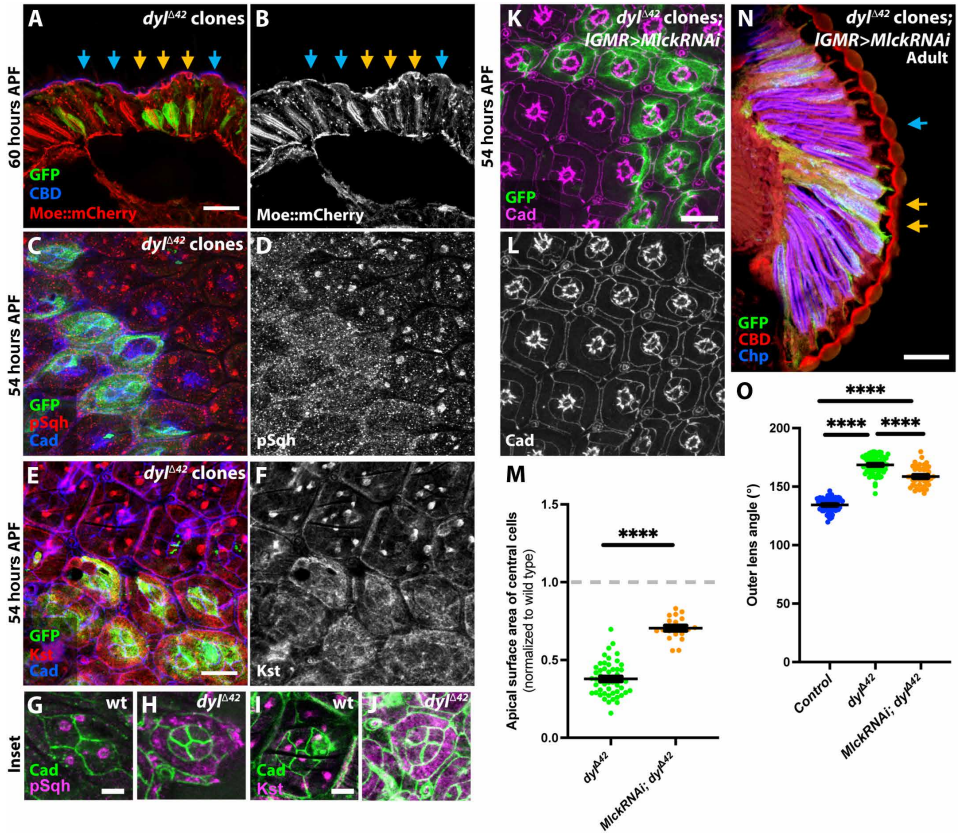

Fig. 3. Loss of *dyl* alters the distribution of cytoskeletal proteins. (**A** and **B**) Cryosection of a 60-hour APF retina showing Moe::mCherry (red) apical accumulation in $dyl^{\Delta 42}$ clones (yellow arrows) marked with GFP (green). Blue arrows, wild-type ommatidia. CBD (blue) labels the corneal lens. (**C** to **J**) Fifty-four-hour APF retinas containing $dyl^{\Delta 42}$ clones (GFP, green), stained with anti-Ecad and anti-Ncad (blue), anti-pSqh [(D), red in (C)], or anti-β_H-spectrin/Kst [(F), red in (E)]. pSqh and β_H-spectrin form foci in wild-type ommatidia, but are diffusely localized in $dyl^{\Delta 42}$ clones. Confocal sections at the apical surfaces of individual wild-type [(G) and (I)] or *dyl* mutant [(H) and (J)] ommatidia labeled with anti-Ecad and anti-Ncad (green) and anti-pSqh [magenta, (G) and (H)] or anti-β_H-spectrin/Kst [magenta, (I) and (J)] show that differences are not due to the more basal position of *dyl* mutant ommatidia. (**K** and **L**) Fifty-four-hour APF retina with $dyl^{\Delta 42}$ clones expressing *UAS-Mlck RNAi* with *IGMR-GAL4*, marked with GFP (green) and stained for Ecad and Ncad [(L), magenta in (K)]. (**M**) Graph of apical surface area of central cells in $dyl^{\Delta 42}$ clones (data from Fig. 2G) and in $dyl^{\Delta 42}$ clones expressing *Mlck RNAi* ($n = 19/8$) normalized to internal control ommatidia ($n = 18/8$) at 54 hours APF. Knocking down *Mlck* partially rescues apical constriction. (**N**) Horizontal cryosection of an adult eye with $dyl^{\Delta 42}$ clones expressing *Mlck RNAi* labeled with GFP (green, yellow arrows), stained with anti-Chp (blue) and CBD (red). Scale bars, 10 μm [(C) to (F) and (K)], 5 μm [(G) to (J)], and 20 μm [(A) and (N)]. (**O**) Graph showing the outer angle between adjacent corneal lenses in control, $dyl^{\Delta 42}$ clones (data from Fig. 1J), and $dyl^{\Delta 42}$ clones expressing *Mlck RNAi* ($n = 41/8$). Knocking down *Mlck* does not restore normal corneal lens curvature. Error bars show mean ± SEM. ****$P < 0.0001$, one-sample *t* test and Wilcoxon test (M) or unpaired two-tailed *t* test with Welch's correction (O).

beta-heavy spectrin (β_H-spectrin) (Fig. 3, E, F, I, and J, and fig. S3, F and G), a component of the spectrin-based membrane cytoskeleton encoded by the gene *karst* (*kst*) that has been reported to control apical cell surface area (*51*). Comparable foci of phospho-Sqh and β_H-spectrin have been observed in cells undergoing pulsatile apical constriction and ratcheting, in the embryonic mesoderm and other contexts (*52*, *53*). Myosin foci are also associated with fluctuations in the area of cone and primary pigment cells as they expand earlier in pupal development (*54*). The lack of such foci in *dyl* mutant cells may indicate that their constriction is a less organized process.

Artificially induced apical constriction alters corneal lens shape

We attempted to test whether apical constriction was necessary for the effect of *dyl* on corneal lens shape by knocking down *Myosin light chain kinase* (*Mlck*), which encodes a kinase that phosphorylates Sqh to induce actomyosin contraction (*55*), in $dyl^{\Delta 42}$ clones. Corneal lens shape was only partially rescued, but because the apical surface area of *dyl* mutant ommatidia was also not fully restored by *Mlck* knockdown, we could not determine whether *dyl* has an effect on corneal lens shape that is independent of apical constriction (Fig. 3, K to O). Knocking down *kst* also partially rescued the apical constriction of *dyl* mutant ommatidia, but did not restore normal corneal lens curvature (fig. S3, H to K). These knockdowns may have been incomplete, or the constriction may be partially independent of Mlck and β_H-spectrin activity. If Dyl-mediated attachments to the aECM exert tension on the apical surfaces of the cone and primary pigment cells to maintain their expansion, then loss of these attachments could result in passive constriction of the apical surfaces.

We next tested whether apical constriction was sufficient to alter corneal lens shape. We artificially induced apical constriction by expressing a constitutively active form of Mlck (*UAS-Mlck*^{CT}) (*56*) with *lGMR-GAL4* in clones in the retina. We confirmed that *Mlck*^{CT}-expressing clones exhibited strong apical constriction in the mid-pupal retina (Fig. 4, A and B). At the adult stage, the overlying

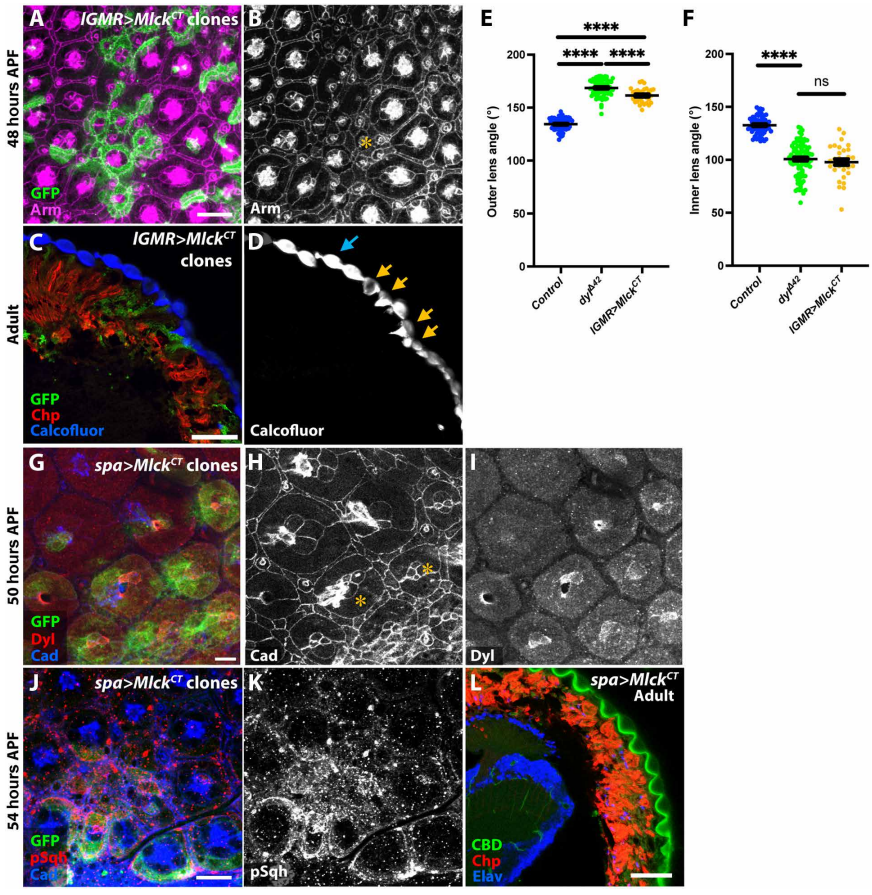

Fig. 4. Apical constriction of central cells is sufficient to alter corneal lens shape. (**A** to **D**) Expression of a constitutively active form of *Mlck* (UAS-*Mlck*^{CT}) in clones marked with GFP (green) in a 48-hour APF pupal retina [(A) and (B)] and adult eye section [(C) and (D)] stained for Arm [(B), magenta in (A)], Chp [red in (C)], and Calcofluor White [(D), blue in (C)]. UAS-*Mlck*^{CT} clones display strong apical constriction of central cells [yellow asterisk, (B)], and in the adult eye, they show distorted corneal lenses with flatter external surfaces and deeper internal curvature [yellow arrows in (D)] than controls (blue arrow). (**E** and **F**) Graphs showing outer angle (E) and inner angle (F) between adjacent corneal lenses in control, $dyl^{\Delta 42}$ clones (data from Fig. 1, J and K), and *Mlck*^{CT} overexpressing clones ($n = 31/5$). Error bars show mean ± SEM. ****$P < 0.0001$, ns $P = 0.369$, unpaired two-tailed *t* test with Welch's correction. (**G** to **K**) UAS-*Mlck*^{CT} expression only in cone and primary pigment cells with *spa-GAL4* in clones marked with GFP (green) at 50 hours APF [(G) to (I)] or 54 hours APF [(J) and (K)]. Retinas are stained with anti-Ecad and anti-Ncad [(H), blue in (G) and (J)], anti-Dyl [(I), red in (G)], and anti-pSqh [(K), red in (J)]. The clones show apical constriction of the central cells and expansion of the lattice cells [asterisks in (H)] and accumulation of disorganized pSqh, but do not affect Dyl expression. (**L**) Horizontal cryosection of an adult eye in which *spa-GAL4* drives *UAS-MLCK*^{CT} in all ommatidia, stained for Chp (red), CBD (green), and the neuronal nuclear marker Elav (blue). CBD staining shows external flattening and deep internal curvature of the corneal lenses. Scale bars, 10 μm [(A), (G), and (J)] and 20 μm [(C) and (L)].

corneal lenses were externally flat with deep and distorted internal curvature (Fig. 4, C to F). Apical constriction in $dyl^{\Delta 42}$ clones is limited to the cone and primary pigment cells (Fig. 2, G and H). Expressing *UAS-Mlck*^{CT} specifically in cone and primary pigment cells with *sparkling-GAL4* (*spa-GAL4*) (*57*) resulted in a change in pSqh distribution and corneal lens shape similar to *dyl* mutant clones, indicating that constriction of these cells is sufficient to alter corneal lens curvature (Fig. 4, G to L). *Mlck*^{CT} expression does not alter the abundance or localization of Dyl (Fig. 4, G to I), confirming that abnormal apical constriction disrupts corneal lens shape even in the presence of Dyl.

Dyl affects the organization of other ZP-domain proteins

The ZP domain is known to mediate homodimerization or heterodimerization, allowing ZP-domain proteins to form extended filaments. Previous studies have shown that the ZP-domain protein Dpy interacts with another ZP-domain protein, Pio, in the epidermis and the lumen of the tracheal system (*32*, *39*). In addition, the ZP-domain protein Quasimodo (Qsm) modifies the strength of the Dpy filaments that connect tendon cells to the external pupal cuticle (*36*). Because Dyl is only transiently expressed in the developing pupal retina, we wondered whether it might interact with other ZP-domain proteins to maintain corneal lens structure. To test this hypothesis, we examined the effect of loss of *dyl* on the organization of Dpy and Pio, which we found to colocalize in the pupal retina (fig. S4, A to D). At 50 hours APF, Dpy and Pio were uniformly localized above the cone and primary pigment cells in both wild-type and $dyl^{\Delta 42}$ ommatidia (Fig. 5, A and B, and fig. S4, E and F). By 54 hours APF, Dpy and Pio were organized into a variety of linear structures above the central region of wild-type ommatidia, but maintained their uniform distribution in $dyl^{\Delta 42}$ clones (Fig. 5, C, D, I, and J). Loss of *dyl* had a similar effect on another ZP-domain protein, Trynity (Tyn) (*42*, *58*) (fig. S4, G to I). These observations suggest that other ZP-domain proteins depend on Dyl for their normal organization.

Tyn, like Dyl, was only detected at mid-pupal stages, but Dpy and Pio were maintained into adulthood. At 60 and 72 hours APF, we found that Dpy and Pio were apical to chitin in the developing corneal lens, and had a less convex shape in $dyl^{\Delta 42}$ clones than in wild-type ommatidia (Fig. 5, E, F, and K). However, when the pseudocone begins to be secreted beneath the corneal lens at 84 hours APF and in the adult eye, Dpy and Pio were lost from the outer surface of the eye and appeared in the pseudocone in both wild-type and *dyl* mutant ommatidia (Fig. 5, G, H, and L). Dpy and Pio are

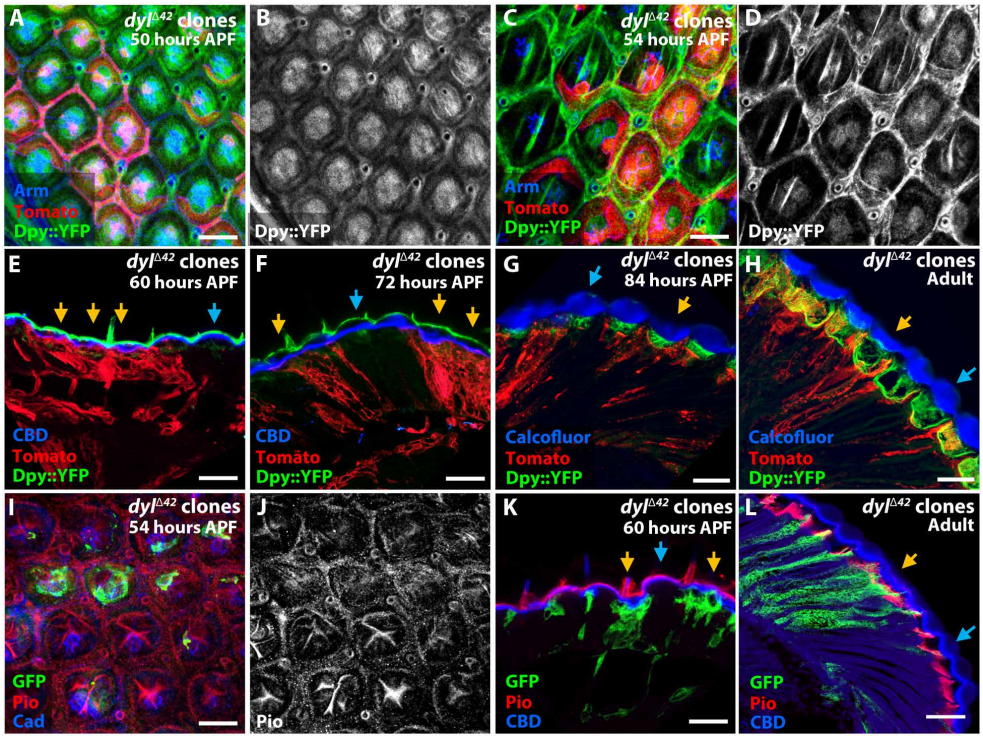

Fig. 5. Loss of *dyl* affects the organization of Dpy and Pio at mid-pupal stages. (**A** to **D**) Pupal retinas at 50 hours APF [(A) and (B)] and 54 hours APF [(C) and (D)] with $dyl^{\Delta 42}$ clones marked by myristoylated Tomato (red), stained for Dpy-YFP [(B) and (D), green in (A) and (C)] and Arm (blue). Dpy-YFP takes on a linear organization that becomes more pronounced at later stages in wild-type but not *dyl* mutant ommatidia. (**E** to **H**) Horizontal sections of retinas containing $dyl^{\Delta 42}$ clones marked by myristoylated Tomato (red) at 60 hours APF (E), 72 hours APF (F), 84 hours APF (G), and adult stage (H), stained for Dpy-YFP (green) and CBD [blue, (E) and (F)] or Calcofluor White (blue, G and H). From 60 to 72 hours APF, Dpy-YFP is present external to the chitin layer of the corneal lenses and is less convex in *dyl* mutant clones (yellow arrows) than wild-type (blue arrows), but at 84 hours APF, it is lost from the external surface and begins to be secreted into the pseudocone under the corneal lens, where it remains in the adult. (**I** to **L**) $dyl^{\Delta 42}$ clones marked with GFP (green) in a 54-hour APF retina [(I) and (J)], and in horizontal cryosections of 60 hours APF (K) and adult (L) retinas, stained for Pio [(J), red in (I), (K), and (L)], Ecad and Ncad [blue in (I)], or CBD [blue in (K) and (L)]. Pio localizes in a similar pattern to Dpy-YFP in pupal retinas and is restricted to the basal part of the pseudocone in adults. Dpy and Pio are also visible in mechanosensory bristles in (E), (F), and (K). Scale bars, 10 μm [(A), (C), and (I)] and 20 μm [(E) to (H), (K), and (L)].

thus in a position to provide outer and inner boundaries for the corneal lens as it is being secreted.

Dpy and Pio are required for normal corneal lens shape

The Dpy protein, the largest isoforms of which have molecular weights close to 2.5 MDa, is known to promote membrane attachment to the cuticle in the embryonic trachea, the pupal wing, and pupal tendon cells, where it forms long filamentous structures (*35*–*37*, *39*, *45*). We hypothesized that Dpy might also contribute to attaching the corneal lens cuticle to the underlying cells. To test this idea, we generated clones homozygous for the lethal allele dpy^{lv1} (*32*) in the retina and examined them at pupal and adult stages. In adults, the overlying corneal lenses showed abnormal and irregular shapes (Fig. 6, C, D, J, and K), comparable to $dyl^{\Delta 42}$ clones. However, *dpy* mutant ommatidia were not shorter on the apical-basal axis (Fig. 6, C and D), consistent with the lack of substantial apical constriction in *dpy* clones earlier in development (Fig. 6, A, B, and I). Clones mutant for the protein null allele pio^{V132} (*32*) (fig. S5, A and B) had little effect on apical constriction (Fig. 6, E, F, and I) and did not alter the external curvature of the corneal lens (Fig. 6, G, H, and J), but showed a deep and distorted inner corneal lens curvature in adults, perhaps indicating that Pio in the pseudocone normally

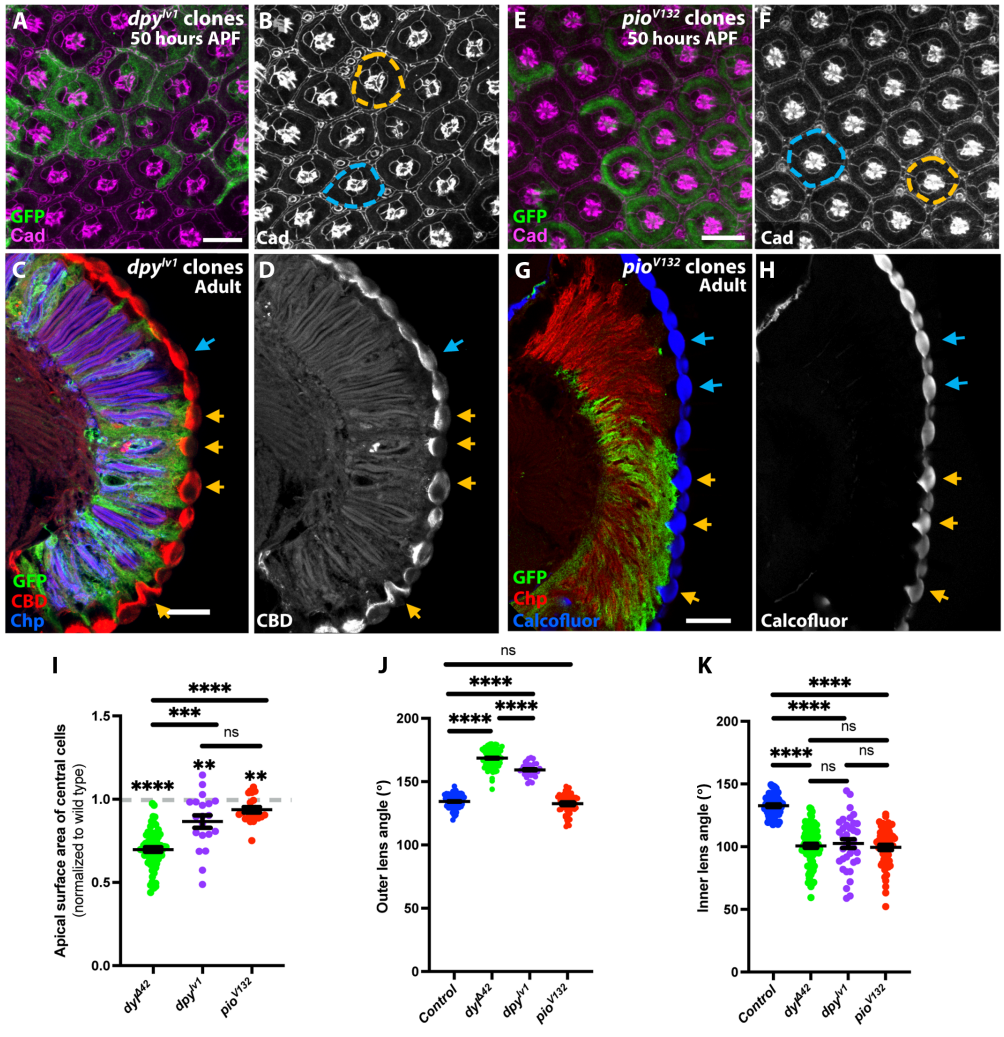

Fig. 6. Loss of *dpy* or *pio* alters corneal lens shape. (**A** to **D**) Fifty hours APF retina [(A) and (B)] and adult eye section [(C) and (D)] containing dpy^{lv1} clones labeled with GFP (green), stained for Ecad and Ncad [(B), magenta in (A)], Chp [blue in (C)], and CBD [(D), red in (C)]. Although dpy^{lv1} clones in the pupal retina show little apical constriction, adult corneal lenses have distorted shapes (yellow arrows) relative to control corneal lenses (blue arrows). (**E** to **H**) Fifty hours APF retina [(E) and (F)] and adult eye section [(G) and (H)] containing pio^{V132} clones labeled with GFP (green), stained for Ecad and Ncad [(F), magenta in (E)], Chp [red in (G)], and Calcofluor White [(H), blue in (G)]. *pio* mutant ommatidia are not apically constricted at 50 hours APF. *pio* mutant corneal lenses have normal outer curvature, but distorted inner curvature (yellow arrows). (**I**) Graph showing the apical surface area of central cells in $dyl^{\Delta 42}$ clones ($n = 73/23$), dpy^{lv1} clones ($n = 22/10$), and pio^{V132} clones ($n = 22/5$) normalized to internal control wild-type ommatidia [$n = 39/23$ (*dyl*), 24/9 (*dpy*), and 9/5 (*pio*)] at 50 hours APF. *dpy* and *pio* mutant ommatidia are much less constricted than *dyl* mutant ommatidia.$^{****}P < 0.0001$, $^{***}P < 0.0003$ ($dyl^{\Delta 42}$ versus dpy^{lv1}), $^{**}P < 0.0020$ (dpy^{lv1}), $^{**}P < 0.0010$ (pio^{V132}), ns $P = 0.0967$ (dpy^{lv1} versus pio^{V132}), one-sample *t* test and Wilcoxon's test. (**J** and **K**) Graphs of the outer angle (J) and inner angle (K) between neighboring corneal lenses in control, $dyl^{\Delta 42}$ clones (data from Fig. 1, J and K), dpy^{lv1} clones ($n = 30/5$), and pio^{V132} clones ($n = 58/8$). $^{****}P < 0.0001$, ns $P = 0.1538$ (J), 0.6419 ($dyl^{\Delta 42}$ versus dpy^{lv1}, K), 0.6217 ($dyl^{\Delta 42}$ versus pio^{V132}, K), 0.4525 (dpy^{lv1} versus pio^{V132}, K), unpaired two-tailed *t* test with Welch's correction. Error bars, mean ± SEM. Scale bars, 10 μm [(A) and (E)] and 20 μm [(C) and (G)].

exerts pressure on the inner surface of the corneal lens (Fig. 6, G, H, and K). *tyn*^{1} (*58*), a protein null allele, did not affect corneal lens shape (fig. S5, C to F). These results indicate that Dpy and Pio organized by Dyl have critical roles in determining corneal lens shape independent of apical cell size.

ZP-domain proteins act as a scaffold to retain chitin

A major component of the corneal lens is chitin, a polymer of N-acetylglucosamine. Chitin assembles into strong fibrillar structures that provide structural integrity (*59*). These chitin polymers are associated with numerous chitin-binding proteins, such as Gasp (*60*), which is highly expressed in the pupal retina (*18*). To examine whether the secretion or arrangement of chitin was affected in *dyl* mutants, we stained *dyl*$^{\Delta 42}$ clones in the pupal retina with a fluorescently labeled CBD probe (*18*). We observed that at 50 hours APF, chitin fibrils were located on the apical surface of wild-type ommatidia, but in *dyl*$^{\Delta 42}$ clones, chitin accumulation was sparse (fig. S6, A and B). At 54 hours APF, high levels of chitin were localized above wild-type ommatidia, but chitin was absent above *dyl* clones and did not appear to be trapped in the secretory pathway within the mutant cells (Fig. 7, A to D). This phenotype could be rescued by expressing a *UAS-dyl* transgene in all retinal cells (fig. S6, O and P). Similarly, Gasp was not observed above *dyl*$^{\Delta 42}$ clones at 54 hours APF (Fig. 7, G and H). *dpy* mutant clones also showed a loss of chitin accumulation (Fig. 7, I and J), despite normal Dyl localization (fig. S6, E and F), but *pio* was not required for chitin retention at this stage (fig. S6, G and H). We first detected chitin above *dyl* clones at 57 hours APF, but at a lower level than in

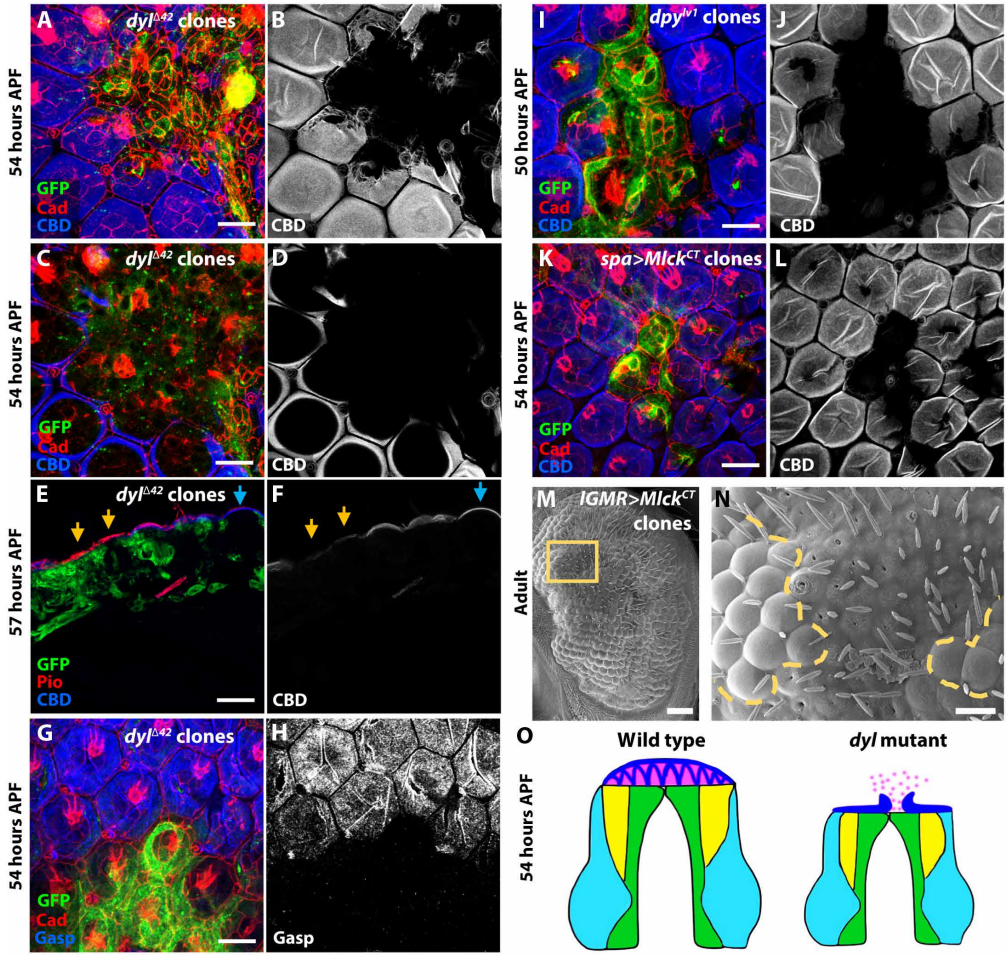

Fig. 7. ZP-domain proteins and apical expansion are necessary for chitin accumulation. (**A** to **H**) Pupal retinas with *dyl*$^{\Delta 42}$ clones marked with GFP (green), stained with CBD [(B), (D), and (F), blue in (A), (C), and (E)] or anti-Gasp [(H), blue in (G)] and anti-Ecad and Ncad [red, (A), (C), and (G)] or anti-Pio [red, (E)] at 54 hours APF [(A) to (D), (G), and (H)] or 57 hours APF [horizontal cryosection, (E) and (F)]. (C) and (D) show a more basal plane of the retina in (A) and (B). At 54 hours APF, chitin and Gasp are absent above *dyl* mutant cells, but intracellular chitin stuck in the secretory pathway is not detected. Chitin begins to appear above *dyl*$^{\Delta 42}$ clones at 57 hours APF, internal to a layer of Pio [yellow arrows, (E) and (F)]. (**I** and **J**) Fifty hours APF pupal retina with *dpy*^{lv1} clones marked by GFP (green) and (**K** and **L**) Fifty-four hours APF retina with *spa-GAL4, UAS-Mlck*^{CT} clones marked by GFP (green), stained with anti-Ecad and Ncad (red) and CBD [(J) and (L), blue in (I) and (K)]. Loss of *dpy* and apical constriction induced by *Mlck*^{CT} result in loss of chitin. (**M** and **N**) Scanning electron micrograph of an eye containing clones expressing *UAS-Mlck*^{CT} with *lGMR-GAL4*. The boxed area is enlarged in (N), and a dashed yellow line indicates the border of the clone. The corneal lenses in *Mlck*^{CT}-expressing ommatidia have flat external surfaces, but there are few gaps in the surface layer. Scale bars, 10 μm [(A), (C), (G), (I), and (K)], 50 μm (M), and 20 μm [(E) and (N)]. (**O**) Model depicting horizontal sections of wild-type and *dyl* mutant ommatidia at 54 hours APF. Chitin (pink) is retained by an external scaffold of proteins including Dpy and Pio (blue) in wild-type ommatidia, but in the absence of Dyl or Dpy, the scaffold is disorganized and chitin diffuses away.

wild-type regions and without the appropriate curvature (Fig. 7, E and F). All these data suggest that ZP-domain proteins are necessary for the timely assembly of chitin in the corneal lens. Expression of the chitin synthase Krotzkopf verkehrt (Kkv) was not reduced in *dyl* mutant ommatidia (fig. S6, C and D), suggesting that *dyl* is not required for the synthesis of chitin, but may restrict its diffusion.

We hypothesize that an external scaffold that includes Dpy and Pio is crucial to retain the nascent chitin layer and mold it into a biconvex shape. Changes in the arrangement of these proteins may allow chitin to diffuse away at the stage when it would normally be deposited (Fig. 7O). This external scaffold is lost, perhaps through proteolytic degradation (*61*, *62*), later in development when the chitinous corneal lens becomes a strong, rigid structure (Fig. 5, G, H, and L). The delay in chitin assembly in *dyl* mutant clones may explain the defects in the surface structure of the adult corneal lens (Fig. 1, A and B).

We observed that chitin was also absent and Dpy was disorganized at 54 hours APF above clones in which apical constriction of cone and primary pigment cells was induced by expressing activated Mlck (Fig. 7, K and L, and fig. S6, M and N). This suggests that the cell shape changes caused by loss of *dyl* may be sufficient to explain the altered ZP-domain scaffold and the lack of chitin retention. It is also possible that direct interactions with Dpy and Pio contribute to the effect of Dyl on their organization, as partially rescuing the constriction defect of *dyl* mutant clones by knocking down *Mlck* failed to rescue Pio organization or chitin accumulation (fig. S6, I to L). In addition, scanning electron micrographs confirmed the flat external surfaces of ommatidia expressing $Mlck^{CT}$ but did not show the extensive surface gaps that were seen in *dyl* mutant clones (Fig. 7, M and N). These results suggest that Dyl assembles a ZP-domain protein structure that prevents dispersal of the components of the developing corneal lens, primarily by maintaining apical expansion of cone and primary pigment cells, but potentially also through an independent mechanism.

DISCUSSION

We show here that forming the precisely curved architecture of the *Drosophila* corneal lens from aECM requires the ZP-domain protein Dyl. Dyl acts transiently at a critical point in development to maintain the apical expansion of corneal lens-secreting cells and to assemble a scaffold containing ZP-domain proteins that acts as a convex outer boundary within which chitin and other corneal lens components are retained. Our results add to a growing body of evidence that the shapes of rigid structures composed of aECM rely on specific sites of attachment to the underlying cells that are mediated by ZP-domain proteins (*35*, *37*, *41*, *42*, *63*, *64*).

Cell shape determines aECM shape

Our data show that the marked apical expansion of primary pigment cells in the pupal retina (*16*, *65*) is essential to build a foundation for corneal lens assembly. Reversing this expansion either by removing Dyl or by activating myosin contraction results in severe corneal lens defects. The apicobasal contraction that occurs in *dyl* mutant or $Mlck^{CT}$-expressing ommatidia places the apical surfaces of cone and primary pigment cells in a more basal position than their wild-type neighbors. If secondary and tertiary pigment cells retain their attachments to the aECM, the ommatidial surface could take on a concave shape, potentially explaining the deeper inner curvature of the overlying corneal lenses (Fig. 2M). The smaller surface area of the central cells could also directly alter the shape of the corneal lens if this structure is assembled one layer at a time, like the tectorial membrane (*66*). Such a pattern of assembly would be consistent with labeling of the outer surface of the early corneal lens and the inner surface of the adult corneal lens by our chitin-binding probe (Fig. 5, K and L), which may preferentially bind to newly deposited chitin. Constriction of the apical cell surface has been shown to produce ridges of aECM in the *C. elegans* cuticle and the *Drosophila* trachea (*12*, *13*); our results suggest that apical expansion can also drive the morphogenesis of specific aECM structures. However, not all aECM remodeling requires cell shape changes; for example, formation of sex-specific pores that accommodate chemosensory cilia in the *C. elegans* cuticle appears to depend on gene expression in the underlying glia rather than on the shape of these cells (*67*).

Dyl stabilizes apical cell expansion

The notable apical constriction of cone and primary pigment cells that we observed in *dyl* mutants implies that Dyl is required to maintain their expanded shape. Dyl is located on the apical surfaces of these cells, and it and other ZP-domain proteins have been shown to attach the plasma membrane to the aECM (*32*, *33*, *38*, *42*, *68*). These attachments can alter cell shape; for instance, apical expansion of cells in the pupal wing is dependent on the ZP-domain proteins Miniature and Dusky (*69*); NOAH-1 and NOAH-2 are required for the concerted cell shape changes that drive elongation of the *C. elegans* embryo (*70*), and Hensin is needed to convert flat β- to columnar α-intercalated cells in the kidney (*71*). The NOAH-1, NOAH-2, and FBN-1 ZP-domain proteins in the embryonic sheath of *C. elegans* resist deformation of the epidermis by mechanical forces (*68*, *70*). We suggest that attachment to the aECM by Dyl enables cone and primary pigment cells to resist mechanical tension exerted by the actomyosin cytoskeleton. Active myosin and β_H-spectrin accumulate in *dyl* mutant cells, and reducing the level of these components partially rescues apical constriction. However, these proteins appear disorganized and do not form foci like those seen in the wild-type cells. Similar foci are associated with changes in apical cell area driven by pulsatile constriction and ratcheting (*52*–*54*), but continuous constriction can occur with a diffuse apical actomyosin distribution, for instance, in boundary larval epithelial cells (*49*, *72*). The loss of apical anchorage may cause *dyl* mutant cells to constrict in a continuous, passive manner that does not involve controlled ratcheting.

Although our electron micrographs suggest that Dyl establishes a physical link between the apical plasma membrane and the aECM, this role at contact sites is surprising because it is likely that the extracellular domain of Dyl is proteolytically cleaved from its transmembrane domain. Overexpressed Dyl appears to diffuse away from the cells that express it (*44*), and Dyl contains a putative furin cleavage site that has been used to enable secretion of a reporter protein (*73*). Nevertheless, loss of *dyl* has cell-autonomous effects on apical constriction and chitin accumulation in the retina (Figs. 2, A to C, and 7, A and B), indicating that the protein does not freely diffuse in this tissue and may associate with other transmembrane proteins and/or with immediately overlying aECM. Alternative explanations for Dyl function are also possible. Rather than directly attaching the membrane to the matrix, Dyl might affect the properties of the developing aECM,

for instance, by endowing it with sufficient tensile strength to counteract cytoskeletal forces that would otherwise drive apical constriction of the cone and pigment cells.

ZP-domain proteins act as a scaffold for chitin retention

Our data also reveal a role for other ZP-domain proteins, including Dpy and Pio, in establishing an external scaffold that helps to shape the corneal lens. Although *dpy* mutant ommatidia show little constriction, indicating that *dpy* acts downstream of or in parallel to the cell shape changes, they fail to accumulate chitin at the normal time and produce deformed corneal lenses. As chitin is not found trapped inside *dyl* or *dpy* mutant cells, it is likely that it diffuses away in the absence of the scaffold. Pio is not necessary to retain chitin at this stage, but it appears to have an analogous role later in development, when it is present in the pseudocone, to maintain the normal curved boundary of the inner surface of the corneal lens (Fig. 6, G and H). Dpy and Pio have a similar function in the trachea, where they provide an elastic structural element of the lumen that controls its shape and size and maintains the chitin matrix (*62*, *74*, *75*). Removal of this structure by proteolysis is necessary for subsequent gas filling of the airway (*61*, *62*), and it is possible that the external corneal lens scaffold is likewise proteolytically degraded in late pupal stages. Transient aECM structures containing ZP-domain proteins also shape many cuticular and tubular structures in *C. elegans* (*7*), and α-tectorin on the surface of supporting cells templates the assembly of collagen fibrils in each layer of the tectorial membrane (*66*).

We find that the arrangement of Dpy and Pio is dependent on Dyl; in wild-type ommatidia, they form linear structures, but this organization is not apparent in *dyl* mutants. We do not know the precise nature of these structures, nor what additional components they may contain. ZP-domain proteins are capable of forming heteropolymeric filaments (*27*–*29*), and another ZP protein, Qsm, is known to promote the secretion and remodeling of Dpy filaments that link tendon cells to the pupal cuticle, increasing their tensile strength (*36*). Because Dyl is only present in the retina for a short time, it may be required to initiate the assembly of a scaffold structure that then becomes self-sustaining. Alternatively, because apical constriction is sufficient to alter Dpy organization and delay chitin accumulation, the role of Dyl may be limited to maintaining apical expansion. Nevertheless, the requirement for *dyl* for normal chitin deposition in bristles and wing hairs (*43*, *44*) suggests that promoting chitin assembly, directly or indirectly, is one of its primary functions.

Other components of the corneal lens may also be affected by loss of *dyl*. Although chitin levels appear normal in sections of adult retinas, scanning electron micrographs show that the external surface of the corneal lens is incomplete. Induced apical constriction does not fully reproduce this loss of surface structure, suggesting that it reflects an independent function of Dyl. In the pupal wing, *dyl* belongs to a cluster of genes with peak expression at 42 hours APF, when the outer envelope layer of the cuticle is being deposited, but it influences the structure of inner layers as well (*64*). *dyl* expression in the embryo is also limited to a short time window in which apical cell remodeling and initial cuticle deposition occur (*42*). Another gene expressed at this time point, *tyn*, is required for the barrier function of the embryonic envelope layer (*58*). It is not clear whether the corneal lens has a typical cuticular envelope, but its outermost layer forms nanostructures composed of the Retinin protein and waxes (*76*). Although *retinin* mRNA is not strongly expressed until very late in pupal development (*77*), its expression is initiated at mid-pupal stages when Dyl is present (*14*). It is possible that Dyl and the Dpy-Pio scaffold also control the retention of Retinin and other components of the outer layer.

In summary, we show here that the development of a biconvex corneal lens depends on both its upper and lower boundaries. The upper boundary, a convex shell of aECM that contains the ZP-domain proteins Dpy and Pio, encloses chitin and its associated proteins as they are secreted by cone and pigment cells. The shape of this shell may be defined by its attachment to the peripheral lattice cells and the pressure exerted on its center by secreted corneal lens components. The lower boundary is the apical plasma membrane of the cone and primary pigment cells. This membrane is flat until pseudocone secretion initiates late in pupal development, and the phenotype of *dyl* mutants suggests that it is maintained taut and expanded by attachment to the aECM. Loss of this expansion or of the pseudocone components Dpy or Pio gives the inner surface of the corneal lens a deeper curvature. It would be interesting to investigate whether mechanical forces exerted on the stromal ECM of the human cornea, perhaps through the ZP-domain proteins ZP4 and endoglin present in the underlying corneal endothelium (*78*, *79*), affect its shape and refractive power (*80*).

MATERIALS AND METHODS

Fly stocks and genetics

Drosophila melanogaster strains were maintained on standard yeast-cornmeal-agar media and raised at 25°C. For analysis of the pupal retina, white prepupae (0 hours APF) were collected with a soft wetted brush and cultured at 25°C until the appropriate developmental stage. Both sexes were used interchangeably for all the experiments, as no sex-specific differences were observed.

D. melanogaster stocks used to generate $dyl^{\Delta 42}$ mutant clones were as follows: (i) *UAS-CD8-GFP, ey3.5-FLP; lGMR-GAL4; FRT 80B, tub-GAL80/TM6B*; (ii) *FRT80B*, $dyl^{\Delta 42}$*/TM6B*; (iii) *Moe::m Cherry; FRT80B*, $dyl^{\Delta 42}$*/SM6-TM6B*; (iv) *Dpy-YFP; FRT80B*, $dyl^{\Delta 42}$*/ SM6-TM6B*; (v) *eyFLP; lGMR-GAL4, UAS-myrTomato; FRT80B, tub-GAL80/TM6B*; (vi) *UAS-dyl; FRT80B*, $dyl^{\Delta 42}$*/TM6B*; (vii) *UAS-kst RNAi; FRT80B*, $dyl^{\Delta 42}$*/SM6-TM6B*; and (viii) *UAS-Mlck RNAi; FRT80B,* $dyl^{\Delta 42}$*/SM6-TM6B*. Stocks used to generate $Mlck^{CT}$ overexpression clones were as follows: (i) *UAS-CD8-GFP, ey3.5-FLP; lGMR-GAL4; FRT42D, tub-GAL80/TM6B*; (ii) *ey3.5-FLP, spa-GA L4; FRT42D, tub-GAL80; UAS-CD8-GFP*; and (iii) *FRT42D; UAS-*$Mlck^{CT}$*/SM6-TM6B*. Stocks that were used to generate dpy^{lv1} mutant clones were as follows: (i) *UAS-CD8-GFP, ey3.5-FLP; FRT40A, tub-GAL80; lGMR-GAL4/TM6B* and (ii) *FRT40A*, dpy^{lv1}*/SM6-TM6B.* Stocks that were used to generate pio^{V132} mutant clones were as follows: (i) *UAS-CD8-GFP, ey3.5-FLP; lGMR-GAL4; FRT42D, tub-GAL80/TM6B* and (ii) *FRT42D*, pio^{V132}*/SM5.* Stocks that were used to generate tyn^{1} mutant clones were as follows: (i) *ey3.5-FLP, FRT19A, tub-GAL80; lGMR-GAL4, UAS-CD8-GFP/SM6-TM6B* and (ii) *FRT19A*, tyn^{1}*/FM7, Tb, Ubi-RFP.*

Stocks were obtained from the following sources: $dyl^{\Delta 42}$, *UAS-dyl* (*42*); tyn^{1} (*58*); *Moe::mCherry P{sChMCA}22* (BL35520), *UAS-Ml* ck^{CT} (BL37527), *UAS-kst RNAi P{TRiP.GLC01654}attP40* (BL50536), dpy^{lv1} (BL278), *FRT42D,* pio^{V132} (BL99937), *spa-GAL4* (BL26656): Bloomington *Drosophila* Stock Center (BDSC); *UAS-Mlck RNAi P{KK113175}VIE-260B*: Vienna *Drosophila* Resource Center (VDRC); and *Dpy-YFP PBac{681.P.FSVS-1}*$dpy^{CPTI001769}$: Kyoto Stock Center.

Immunohistochemistry

For cryosectioning, adult or pupal heads with the proboscis removed were glued onto glass rods using nail polish and fixed for 4 hours in 4% formaldehyde in 0.2 M sodium phosphate buffer (PB), pH 7.2, at 4°C. The heads were then incubated through an increasing gradient of sucrose in PB (5, 10, 25, and 30% sucrose) for 20 min each, transferred to plastic molds containing optimal cutting temperature (OCT) compound and frozen on dry ice. Cryosections of 12 μm were cut at −21°C, transferred onto positively charged slides, and postfixed in 0.5% formaldehyde in PB at room temperature (RT) for 30 min. The slides were then washed in phosphate-buffered saline (PBS) with 0.3% Triton X-100 (PBT) three times for 10 min each, blocked for 1 hour at RT in 1% bovine serum albumin (BSA) in PBT, and incubated in primary antibodies overnight at 4°C in PBT/1% BSA. After three 20-min washes in PBT, slides were incubated in secondary antibodies in PBT/1% BSA for 2 hours at RT and mounted in Fluoromount-G (Southern Biotech). A 1:5 dilution of Calcofluor White solution (25% in water; Sigma-Aldrich, 910090) was included with the secondary antibodies where indicated.

Pupal retinas attached to the brain were dissected from staged pupae and collected in ice-cold PBS in a glass plate. These samples were fixed on ice in 4% formaldehyde in PBS for 30 min. The samples were washed three times for 10 min each in PBT and incubated overnight at 4°C in primary antibodies in 10% donkey serum in PBT. After three 20-min washes in PBT, the samples were incubated for 2 hours in secondary antibodies in PBT/10% serum at RT, and washed again three times for 20 min in PBT. Last, the retinas were separated from the brain and mounted in 80% glycerol in PBS.

The primary antibodies used were as follows: mouse anti-Chp [1:50; Developmental Studies Hybridoma Bank (DSHB), 24B10], chicken anti-GFP (1:400; Thermo Fisher Scientific, A-10262), rat anti-Elav (1:100; DSHB, Rat-Elav-7E8A10), rat anti-Ecad (1:10, DSHB, DCAD2), mouse anti-Gasp (1:20, DSHB, 2A12), rabbit anti-Dyl (1:300) (*42*), rat anti-Tyn (1:100) (*42*), rabbit anti-Pio (1:300) (*39*), guinea pig anti-pSqh (1:1000) (*50*), rabbit anti-Kkv (1:100) (*81*), and rabbit anti–β_H-spectrin (1:5000) (*82*). All antibodies were validated either using mutant or knockdown conditions as shown or by verifying that the staining pattern matched previously published descriptions. The secondary antibodies used were from either Jackson ImmunoResearch (Cy3 or Cy5 conjugates used at 1:200) or Invitrogen (Alexa488 conjugates used at 1:1000). Fluorescently labeled SNAP-CBD-probes (1:200) (*18*) were included with the secondary antibodies. Images were acquired on a Leica SP8 confocal microscope with a 63× oil immersion lens and processed using ImageJ and Adobe Photoshop.

Electron microscopy

For transmission electron microscopy, adult heads cut in half or whole 72 hours APF pupal heads removed from the body were incubated in freshly made fixative containing 2.5% glutaraldehyde, 2% paraformaldehyde, and 0.05% Triton X-100 in 0.1 M sodium cacodylate buffer (CB), pH 7.2, on a rotator for at least 4 hours until all heads had sunk to the bottom of the tube, and then in the same fixative without Triton X-100 overnight at 4°C on a rotator. After washing three times for 10 min in CB, the heads were postfixed in 1% OsO_4 in CB for 1.5 hours, washed three times for 10 min in water, dehydrated in an ethanol series (30, 50, 70, 85, 95, and 100%), rinsed twice with propylene oxide, and embedded in EMbed812 epoxy resin (Electron Microscopy Sciences). Ultrathin sections (70 nm) were cut and mounted on formvar-coated slot grids and stained with uranyl acetate and lead citrate (*83*). Electron microscopy imaging was performed on a Talos120C transmission electron microscope (Thermo Fisher Scientific) and recorded using a Gatan (4k × 4k) OneView Camera with Digital Micrograph software (Gatan).

For scanning electron microscopy, whole flies were fixed for 2 hours at room temperature and then overnight at 4°C in 1% glutaraldehyde/1% formaldehyde/0.2% Triton X-100/0.1 M sodium cacodylate, pH 7.2. After three 10-min washes in PBS, the flies were postfixed in 1% OsO_4 in CB for 1 hour and rinsed three times for 10 min in water. They were dehydrated in an ethanol series (30, 50, 70, 85, 95, and 3× 100%) and stored in 100% ethanol overnight. The eyes were critical point dried using a Tousimis Autosamdri-931 critical point dryer (Tousimis, Rockville, MD), mounted on SEM stubs covered with double-sided electron-conductive tape, coated with gold/palladium by a Safematic CCU-010 SEM coating system (Rave Scientific, Somerset, NJ), and imaged on a Zeiss Gemini300 FESEM (Carl Zeiss Microscopy, Oberkochen, Germany) using a secondary electron detector (SE_2) at 5 kV with a working distance (WD) between 15.2 and 19.4 mm.

Quantification and statistical analysis

The outer and inner angles between adjacent corneal lenses were measured according to the schematic in Fig. 1E, using the angle tool in ImageJ. To measure the apical surface areas of ommatidia and central cells, ROI were drawn and measured in ImageJ using the freehand selection tool in Z-projections that included the apical surface of the retina. Areas of mutant ommatidia were normalized to the average area of wild-type ommatidia from the same retina. To measure ommatidial height, freehand straight lines were drawn from the corneal lens surface to the base of the rhabdomere using the line tool in ImageJ and measured. Values were plotted in GraphPad Prism v10. Significance was calculated using a one-sample *t* test and Wilcoxon's test or Welch's two-tailed unpaired *t* test. Sample numbers and definitions of error bars are given in the figure legends. Sample sizes for quantifications were not predefined and no samples were excluded.

Supplementary Materials

This PDF file includes:

Figs. S1 to S6

Legend for data S1

Other Supplementary Material for this manuscript includes the following:

Data S1

REFERENCES AND NOTES

1. N. V. Popova, M. Juecker, The functional role of extracellular matrix proteins in cancer. *Cancer* **14**, 238 (2022).
2. L. Arseni, A. Lombardi, D. Orioli, From structure to phenotype: Impact of collagen alterations on human health. *Int. J. Mol. Sci.* **19**, 1407 (2018).
3. A. Pozzi, P. D. Yurchenco, R. V. Lozzo, The nature and biology of basement membranes. *Matrix Biol.* **57–58**, 1–11 (2017).
4. N. H. Brown, Extracellular matrix in development: Insights from mechanisms conserved between invertebrates and vertebrates. *Cold Spring Harb. Perspect Biol.* **3**, a005082 (2011).
5. D. A. C. Walma, K. M. Yamada, The extracellular matrix in development. *Development* **147**, dev175596 (2020).
6. S. Li Zheng, J. G. Adams, A. D. Chisholm, Form and function of the apical extracellular matrix: New insights from *Caenorhabditis elegans*, *Drosophila melanogaster*, and the vertebrate inner ear. *Fac. Rev.* **9**, 27 (2020).
7. J. D. Cohen, M. V. Sundaram, *C. elegans* apical extracellular matrices shape epithelia. *J. Dev. Biol.* **8**, 23 (2020).

8. A. Milusev, R. Rieben, N. Sorvillo, The endothelial glycocalyx: A possible therapeutic target in cardiovascular disorders. *Front. Cardiovasc. Med.* **9**, 897087 (2022).
9. R. J. Goodyear, G. P. Richardson, Structure, function, and development of the tectorial membrane: An extracellular matrix essential for hearing. *Curr. Top. Dev. Biol.* **130**, 217–244 (2018).
10. M. Yamaguchi, K. Yamamoto, Mucin glycans and their degradation by gut microbiota. *Glycoconj. J.* **40**, 493–512 (2023).
11. J. Perez-Gil, Structure of pulmonary surfactant membranes and films: The role of proteins and lipid-protein interactions. *Biochim. Biophys. Acta* **1778**, 1676–1695 (2008).
12. A. Ozturk-Colak, B. Moussian, S. J. Araujo, J. Casanova, A feedback mechanism converts individual cell features into a supracellular ECM structure in *Drosophila* trachea. *eLife* **5**, e09373 (2016).
13. S. S. Katz, T. J. Barker, H. M. Maul-Newby, A. P. Sparacio, K. C. Q. Nguyen, C. L. Maybrun, A. Belfi, J. D. Cohen, D. H. Hall, M. V. Sundaram, A. R. Frand, A transient apical extracellular matrix relays cytoskeletal patterns to shape permanent acellular ridges on the surface of adult *C. elegans*. *PLoS Genet.* **18**, e1010348 (2022).
14. A. L. Stahl, M. Charlton-Perkins, E. K. Buschbeck, T. A. Cook, The cuticular nature of corneal lenses in *Drosophila melanogaster*. *Dev. Genes Evol.* **227**, 271–278 (2017).
15. M. Charlton-Perkins, T. A. Cook, Building a fly eye: Terminal differentiation events of the retina, corneal lens, and pigmented epithelia. *Curr. Top. Dev. Biol.* **93**, 129–173 (2010).
16. R. L. Cagan, D. F. Ready, The emergence of order in the *Drosophila* pupal retina. *Dev. Biol.* **136**, 346–362 (1989).
17. M. A. Charlton-Perkins, E. D. Sendler, E. K. Buschbeck, T. A. Cook, Multifunctional glial support by Semper cells in the *Drosophila* retina. *PLoS Genet.* **13**, e1006782 (2017).
18. H. Wang, C. A. Morrison, N. Ghosh, J. S. Tea, G. B. Call, J. E. Treisman, The Blimp-1 transcription factor acts in non-neuronal cells to regulate terminal differentiation of the *Drosophila* eye. *Development* **149**, dev200217 (2022).
19. S. Plaza, H. Chanut-Delalande, I. Fernandes, P. M. Wassarman, F. Payre, From A to Z: Apical structures and zona pellucida-domain proteins. *Trends Cell Biol.* **20**, 524–532 (2010).
20. P. M. Wassarman, E. S. Litscher, Zona pellucida genes and proteins: Essential players in mammalian oogenesis and fertility. *Genes-Basel* **12**, 1266 (2021).
21. K. Nishimura, E. Dioguardi, S. Nishio, A. Villa, L. Han, T. Matsuda, L. Jovine, Molecular basis of egg coat cross-linking sheds light on ZP1-associated female infertility. *Nat. Commun.* **10**, 3086 (2019).
22. M. Renner, G. Bergmann, I. Krebs, C. End, S. Lyer, F. Hilberg, B. Helmke, N. Gassler, F. Autschbach, F. Bikker, O. Strobel-Freidekind, S. Gronert-Sum, A. Benner, S. Blaich, R. Wittig, M. Hudler, A. J. Ligtenberg, J. Madsen, U. Holmskov, V. Annese, A. Latiano, P. Schirmacher, A. V. N. Amerongen, M. D'Amato, P. Kioschis, M. Hafner, A. Poustka, J. Mollenhauer, DMBT1 confers mucosal protection in vivo and a deletion variant is associated with Crohn's disease. *Gastroenterology* **133**, 1499–1509 (2007).
23. K. A. Mcallister, K. M. Grogg, D. W. Johnson, C. J. Gallione, M. A. Baldwin, C. E. Jackson, E. A. Helmbold, D. S. Markel, W. C. Mckinnon, J. Murrell, M. K. Mccormick, M. A. Pericakvance, P. Heutink, B. A. Oostra, T. Haitjema, C. J. J. Westerman, M. E. Porteous, A. E. Guttmacher, M. Letarte, D. A. Marchuk, Endoglin, a TGF-β binding protein of endothelial cells, is the gene for hereditary haemorrhagic telangiectasia type 1. *Nat. Genet.* **8**, 345–351 (1994).
24. E. Wheeler, S. Thomas, Diagnosis and long-term management of uromodulin kidney disease. *Cureus J. Med. Sci.* **11**, e4720 (2019).
25. K. Verhoeven, L. Van Laer, K. Kirschhofer, P. K. Legan, D. C. Hughes, I. Schatteman, M. Verstreken, P. Van Hauwe, P. Coucke, A. Chen, R. J. H. Smith, T. Somers, F. E. Offeciers, P. Van de Heyning, G. P. Richardson, F. Wachtler, W. T. Kimberling, P. J. Willems, P. J. Govaerts, G. Van Camp, Mutations in the human *alpha-tectorin* gene cause autosomal dominant non-syndromic hearing impairment. *Nat. Genet.* **19**, 60–62 (1998).
26. S. Vijayakumar, J. Takito, X. Gao, G. J. Schwartz, Q. Al-Awqati, Differentiation of columnar epithelia: The hensin pathway. *J. Cell Sci.* **119**, 4797–4801 (2006).
27. M. Bokhove, L. Jovine, Structure of zona pellucida module proteins. *Curr. Top. Dev. Biol.* **130**, 413–442 (2018).
28. L. Jovine, H. Y. Qi, Z. Williams, E. Litscher, P. M. Wassarman, The ZP domain is a conserved module for polymerization of extracellular proteins. *Nat. Cell Biol.* **4**, 457–461 (2002).
29. A. Stsiapanava, C. Xu, M. Brunati, S. Zamora-Caballero, C. Schaeffer, M. Bokhove, L. Han, H. Hebert, M. Carroni, S. Yasumasu, L. Rampoldi, B. Wu, L. Jovine, Cryo-EM structure of native human uromodulin, a zona pellucida module polymer. *EMBO J.* **39**, e106807 (2020).
30. Z. Williams, P. M. Wassarman, Secretion of mouse ZP3, the sperm receptor, requires cleavage of its polypeptide at a consensus furin cleavage-site. *Biochemistry* **40**, 929–937 (2001).
31. J. J. Stanisich, D. S. Zyla, P. Afanasyev, J. Xu, A. Kipp, E. Olinger, O. Devuyst, M. Pilhofer, D. Boehringer, R. Glockshuber, The cryo-EM structure of the human uromodulin filament core reveals a unique assembly mechanism. *eLife* **9**, e60265 (2020).
32. C. Bokel, A. Prokop, N. H. Brown, Papillote and Piopio: *Drosophila* ZP-domain proteins required for cell adhesion to the apical extracellular matrix and microtubule organization. *J. Cell Sci.* **118**, 633–642 (2005).
33. M. G. Heiman, S. Shaham, DEX-1 and DYF-7 establish sensory dendrite length by anchoring dendritic tips during cell migration. *Cell* **137**, 344–355 (2009).
34. P. K. Legan, V. A. Lukashkina, R. J. Goodyear, M. Kossi, I. J. Russell, G. P. Richardson, A targeted deletion in alpha-tectorin reveals that the tectorial membrane is required for the gain and timing of cochlear feedback. *Neuron* **28**, 273–285 (2000).
35. R. P. Ray, A. Matamoro-Vidal, P. S. Ribeiro, N. Tapon, D. Houle, I. Salazar-Ciudad, B. J. Thompson, Patterned anchorage to the apical extracellular matrix defines tissue shape in the developing appendages of *Drosophila*. *Dev. Cell* **34**, 310–322 (2015).
36. W. C. Chu, S. Hayashi, Mechano-chemical enforcement of tendon apical ECM into nano-filaments during *Drosophila* flight muscle development. *Curr. Biol.* **31**, 1366–1378. e7 (2021).
37. A. Tsuboi, K. Fujimoto, T. Kondo, Spatiotemporal remodeling of extracellular matrix orients epithelial sheet folding. *Sci. Adv.* **9**, eadh2154 (2023).
38. Y. D. Chung, J. Zhu, Y. Han, M. J. Kernan, *nompA* encodes a PNS-specific, ZP domain protein required to connect mechanosensory dendrites to sensory structures. *Neuron* **29**, 415–428 (2001).
39. A. Jazwinska, C. Ribeiro, M. Affolter, Epithelial tube morphogenesis during *Drosophila* tracheal development requires Piopio, a luminal ZP protein. *Nat. Cell Biol.* **5**, 895–901 (2003).
40. H. K. Gill, J. D. Cohen, J. Ayala-Figueroa, R. Forman-Rubinsky, C. Poggioli, K. Bickard, J. M. Parry, P. Pu, D. H. Hall, M. V. Sundaram, Integrity of narrow epithelial tubes in the *C. elegans* excretory system requires a transient luminal matrix. *PLoS Genet.* **12**, e1006205 (2016).
41. J. D. Cohen, A. P. Sparacio, A. C. Belfi, R. Forman-Rubinsky, D. H. Hall, H. Maul-Newby, A. R. Frand, M. V. Sundaram, A multi-layered and dynamic apical extracellular matrix shapes the vulva lumen in *Caenorhabditis elegans*. *eLife* **9**, e57874 (2020).
42. I. Fernandes, H. Chanut-Delalande, P. Ferrer, Y. Latapie, L. Waltzer, M. Affolter, F. Payre, S. Plaza, Zona pellucida domain proteins remodel the apical compartment for localized cell shape changes. *Dev. Cell* **18**, 64–76 (2010).
43. R. Nagaraj, P. N. Adler, Dusky-like functions as a Rab11 effector for the deposition of cuticle during *Drosophila* bristle development. *Development* **139**, 906–916 (2012).
44. P. N. Adler, L. F. Sobala, D. Thom, R. Nagaraj, *dusky-like* is required to maintain the integrity and planar cell polarity of hairs during the development of the *Drosophila* wing. *Dev. Biol.* **379**, 76–91 (2013).
45. M. B. Wilkin, M. N. Becker, D. Mulvey, I. Phan, A. Chao, K. Cooper, H. J. Chung, I. D. Campbell, M. Baron, R. MacIntyre, *Drosophila* Dumpy is a gigantic extracellular protein required to maintain tension at epidermal-cuticle attachment sites. *Curr. Biol.* **10**, 559–567 (2000).
46. M. F. Wernet, T. Labhart, F. Baumann, E. O. Mazzoni, F. Pichaud, C. Desplan, Homothorax switches function of *Drosophila* photoreceptors from color to polarized light sensors. *Cell* **115**, 267–279 (2003).
47. B. R. Graveley, A. N. Brooks, J. W. Carlson, M. O. Duff, J. M. Landolin, L. Yang, C. G. Artieri, M. J. van Baren, N. Boley, B. W. Booth, J. B. Brown, L. Cherbas, C. A. Davis, A. Dobin, R. Li, W. Lin, J. H. Malone, N. R. Mattiuzzo, D. Miller, D. Sturgill, B. B. Tuch, C. Zaleski, D. Zhang, M. Blanchette, S. Dudoit, B. Eads, R. E. Green, A. Hammonds, L. Jiang, P. Kapranov, L. Langton, N. Perrimon, J. E. Sandler, K. H. Wan, A. Willingham, Y. Zhang, Y. Zou, J. Andrews, P. J. Bickel, S. E. Brenner, M. R. Brent, P. Cherbas, T. R. Gingeras, R. A. Hoskins, T. C. Kaufman, B. Oliver, S. E. Celniker, The developmental transcriptome of *Drosophila melanogaster*. *Nature* **471**, 473–479 (2011).
48. C. Polesello, I. Delon, P. Valenti, P. Ferrer, F. Payre, Dmoesin controls actin-based cell shape and polarity during *Drosophila melanogaster* oogenesis. *Nat. Cell Biol.* **4**, 782–789 (2002).
49. C. G. Vasquez, M. Tworoger, A. C. Martin, Dynamic myosin phosphorylation regulates contractile pulses and tissue integrity during epithelial morphogenesis. *J. Cell Biol.* **206**, 435–450 (2014).
50. L. Zhang, R. E. Ward, Distinct tissue distributions and subcellular localizations of differently phosphorylated forms of the myosin regulatory light chain in *Drosophila*. *Gene Expr. Patterns* **11**, 93–104 (2011).
51. H. Deng, W. Wang, J. Z. Yu, Y. G. Zheng, Y. Qing, D. J. Pan, Spectrin regulates Hippo signaling by modulating cortical actomyosin activity. *eLife* **4**, e06567 (2015).
52. R. Levayer, T. Lecuit, Biomechanical regulation of contractility: Spatial control and dynamics. *Trends Cell Biol.* **22**, 61–81 (2012).
53. D. Krueger, C. P. Cartes, T. Makaske, S. De Renzis, β_H-spectrin is required for ratcheting apical pulsatile constrictions during tissue invagination. *EMBO Rep.* **21**, e49858 (2020).
54. L. Blackie, R. F. Walther, M. F. Staddon, S. Banerjee, F. Pichaud, Cell-type-specific mechanical response and myosin dynamics during retinal lens development in *Drosophila*. *Mol. Biol. Cell* **31**, 1355–1369 (2020).
55. S. I. Kojima, M. Mishima, I. Mabuchi, Y. Hotta, A single *Drosophila melanogaster myosin light chain kinase* gene produces multiple isoforms whose activities are differently regulated. *Genes Cells* **1**, 855–871 (1996).
56. Y. S. Kim, J. L. Fritz, A. K. Seneviratne, M. F. A. VanBerkum, Constitutively active Myosin light chain kinase alters axon guidance decisions in *Drosophila* embryos. *Dev. Biol.* **249**, 367–381 (2002).

57. R. Jiao, M. Daube, H. Duan, Y. Zou, E. Frei, M. Noll, Headless flies generated by developmental pathway interference. *Development* **128**, 3307–3319 (2001).
58. Y. Itakura, S. Inagaki, H. Wada, S. Hayashi, Trynity controls epidermal barrier function and respiratory tube maturation in *Drosophila* by modulating apical extracellular matrix nano-patterning. *PLoS ONE* **13**, e0209058 (2018).
59. J. Hou, B. E. Aydemir, A. G. Dumanli, Understanding the structural diversity of chitins as a versatile biomaterial. *Philos. Trans. A Math. Phys. Eng. Sci.* **379**, 20200331 (2021).
60. K. Tiklova, V. Tsarouhas, C. Samakovlis, Control of airway tube diameter and integrity by secreted chitin-binding proteins in *Drosophila*. *PLoS ONE* **8**, e67415 (2013).
61. L. Drees, T. Konigsmann, M. H. J. Jaspers, R. Pflanz, D. Riedel, R. Schuh, Conserved function of the matriptase-prostasin proteolytic cascade during epithelial morphogenesis. *PLoS Genet.* **15**, e1007882 (2019).
62. L. Drees, S. Schneider, D. Riedel, R. Schuh, M. Behr, The proteolysis of ZP proteins is essential to control cell membrane structure and integrity of developing tracheal tubes in *Drosophila*. *eLife* **12**, e91079 (2023).
63. R. Gueta, J. Levitt, A. Xia, O. Katz, J. S. Oghalai, I. Rousso, Structural and mechanical analysis of tectorial membrane *Tecta* mutants. *Biophys. J.* **100**, 2530–2538 (2011).
64. L. F. Sobala, P. N. Adler, The gene expression program for the formation of wing cuticle in *Drosophila*. *PLoS Genet.* **12**, e1006100 (2016).
65. D. E. Larson, R. I. Johnson, M. Swat, J. B. Cordero, J. A. Glazier, R. L. Cagan, Computer simulation of cellular patterning within the *Drosophila* pupal eye. *PLoS Comput. Biol.* **6**, e1000841 (2010).
66. D. K. Kim, J. A. Kim, J. Park, A. Niazi, A. Almishaal, S. Park, The release of surface-anchored α-tectorin, an apical extracellular matrix protein, mediates tectorial membrane organization. *Sci. Adv.* **5**, eaay6300 (2019).
67. W. Fung, T. M. Tan, I. Kolotuev, M. G. Heiman, A sex-specific switch in a single glial cell patterns the apical extracellular matrix. *Curr. Biol.* **33**, 4174–4186.e7 (2023).
68. M. Kelley, J. Yochem, M. Krieg, A. Calixto, M. G. Heiman, A. Kuzmanov, V. Meli, M. Chalfie, M. B. Goodman, S. Shaham, A. Frand, D. S. Fay, FBN-1, a fibrillin-related protein, is required for resistance of the epidermis to mechanical deformation during *C. elegans* embryogenesis. *eLife* **4**, e06565 (2015).
69. F. Roch, C. R. Alonso, M. Akam, *Drosophila miniature* and *dusky* encode ZP proteins required for cytoskeletal reorganisation during wing morphogenesis. *J. Cell Sci.* **116**, 1199–1207 (2003).
70. T. T. K. Vuong-Brender, S. K. Suman, M. Labouesse, The apical ECM preserves embryonic integrity and distributes mechanical stress during morphogenesis. *Development* **144**, 4336–4349 (2017).
71. X. B. Gao, D. Eladari, F. Leviel, B. Y. Tew, C. Miro-Julia, F. Cheema, L. Miller, R. Nelson, T. G. Paunescu, M. McKee, D. Brown, Q. Al-Awqati, Deletion of hensin/DMBT1 blocks conversion of beta- to alpha-intercalated cells and induces distal renal tubular acidosis. *Proc. Natl. Acad. Sci. U.S.A.* **107**, 21872–21877 (2010).
72. P. Pulido Companys, A. Norris, M. Bischoff, Coordination of cytoskeletal dynamics and cell behaviour during *Drosophila* abdominal morphogenesis. *J. Cell Sci.* **133**, jcs235325 (2020).
73. L. F. Sobala, Y. Wang, P. N. Adler, ChtVis-Tomato, a genetic reporter for in vivo visualization of chitin deposition in *Drosophila*. *Development* **142**, 3974–3981 (2015).
74. A. Jazwinska, M. Affolter, A family of genes encoding zona pellucida (ZP) domain proteins is expressed in various epithelial tissues during *Drosophila* embryogenesis. *Gene Expr. Patterns* **4**, 413–421 (2004).
75. B. Dong, E. Hannezo, S. Hayashi, Balance between apical membrane growth and luminal matrix resistance determines epithelial tubule shape. *Cell Rep.* **7**, 941–950 (2014).
76. M. Kryuchkov, O. Bilousov, J. Lehmann, M. Fiebig, V. L. Katanaev, Reverse and forward engineering of *Drosophila* corneal nanocoatings. *Nature* **585**, 383–389 (2020).
77. E. Kim, Y. Choi, S. Lee, Y. Seo, J. Yoon, K. Baek, Characterization of the *Drosophila melanogaster retinin* gene encoding a cornea-specific protein. *Insect Mol. Biol.* **17**, 537–543 (2008).
78. M. Yoshihara, H. Ohmiya, S. Hara, S. Kawasaki, FANTOM consortium, Y. Hayashizaki, M. Itoh, H. Kawaji, M. Tsujikawa, K. Nishida, Discovery of molecular markers to discriminate corneal endothelial cells in the human body. *PLoS ONE* **10**, e0117581 (2015).
79. Y. Motegi, T. Usui, K. Ishida, S. Kato, H. Yamashita, Regulation of bovine corneal endothelial cell cycle by transforming growth factor-beta. *Acta Ophthalmol. Scand.* **81**, 517–525 (2003).
80. R. Zhang, B. Li, H. Li, Extracellular matrix mechanics regulate the ocular physiological and pathological activities. *J. Ophthalmol.* **2023**, 7626920 (2023).
81. E. De Giorgio, P. Giannios, M. L. Espinas, M. Llimargas, A dynamic interplay between chitin synthase and the proteins Expansion/Rebuf reveals that chitin polymerisation and translocation are uncoupled in *Drosophila*. *PLoS Biol.* **21**, e3001978 (2023).
82. N. Pogodalla, H. Kranenburg, S. Rey, S. Rodrigues, A. Cardona, C. Klambt, *Drosophila* $ß_{Heavy}$-Spectrin is required in polarized ensheathing glia that form a diffusion-barrier around the neuropil. *Nat. Commun.* **12**, 6357 (2021).
83. M. W. Hess, K. Pfaller, B. Hampolz, S. Longato, D. Teis, A. Florl, K. Gutleben, L. A. Huber, Microscopy of the *Drosophila* facet eye: Vademecum for standardized fixation, embedding, and sectioning. *Microsc. Res. Tech.* **69**, 93–98 (2006).

Acknowledgments: We thank M. Affolter, S. Hayashi, C. Klämbt, M. Llimargas, F. Payre, R. Ward, the Bloomington *Drosophila* stock center, the Vienna *Drosophila* resource center, the Kyoto stock center, and the Developmental Studies Hybridoma Bank for fly stocks and reagents. Information available on FlyBase was invaluable for this work. We thank NYULH DART Microscopy Laboratory members A. F.-X. Liang, J. Sall, J. Liang, and C. Petzold for consultation and assistance with plastic sections and electron microscopy. This core is partially funded by NYU Cancer Center Support Grant NIH/NCI P30CA016087, and the Gemini300 FESEM was supported by NIH S10 OD019974. We thank D. Gandhi, S. Khan, and G. Jang for technical assistance. The manuscript was improved by the critical comments of G. Bhabha, M. Bustillo, H. Knaut, S. Nair, and H. Wang. **Funding:** This work was supported by National Institutes of Health grant R01EY032896 to J.E.T. **Author contributions:** Conceptualization: N.G. and J.E.T. Data curation: N.G. and J.E.T. Formal analysis: N.G. Funding acquisition: J.E.T. Investigation: N.G. Methodology: N.G. Project administration: N.G. and J.E.T. Resources: N.G. and J.E.T. Supervision: N.G. and J.E.T. Validation: N.G. and J.E.T. Visualization: N.G. and J.E.T. Writing—original draft: N.G. Writing—review and editing: N.G. and J.E.T. **Competing interests:** The authors declare that they have no competing interests. **Data and materials availability:** All data needed to evaluate the conclusions in the paper are present in the paper and/or the Supplementary Materials.

Submitted 31 January 2024
Accepted 11 July 2024
Published 21 August 2024
10.1126/sciadv.ado4167